The Canadian Mineralogist
Vol. 43, pp. 1315-1329 (2005)

AGE AND SIGNIFICANCE OF RUBY-BEARING MARBLE FROM THE RED RIVER SHEAR ZONE, NORTHERN VIETNAM

VIRGINIE GARNIER§ AND DANIEL OHNENSTETTER

CRPG–CNRS, UPR 2300, 15, rue Notre-Dame des Pauvres, BP 20, F–54501 Vandœuvre-lès-Nancy, France

GASTON GIULIANI

IRD, Département ME, UR 154, LMTG – Toulouse, and CRPG–CNRS, UPR2300, 15, rue Notre-Dame des Pauvres, BP 20, F–54501 Vandœuvre-lès-Nancy, France

HENRI MALUSKI

Laboratoire de Géochronologie, Institut des Sciences de la Terre, de l'Eau et de l'Espace de Montpellier, Université de Montpellier, 2, Place Eugène Bataillon, F–34095 Montpellier, France

ETIENNE DELOULE

CRPG–CNRS, UPR 2300, 15, rue Notre-Dame des Pauvres, BP 20, F–54501 Vandœuvre-lès-Nancy, France

TRINH PHAN TRONG

Institute of Geological Sciences, CNST, Nghia Dô, Câu Giây, Hanoi, Vietnam

LONG PHAM VAN

Vietnam National Gem and Gold Corporation, 91 Dinh Tien Hoang Street, Hanoi, Vietnam

VINH HOÀNG QUANG

Institute of Geological Sciences, CNST, Nghia Dô, Câu Giây, Hanoi, Vietnam

ABSTRACT

Marble-hosted ruby deposits occur in the Lo Gam tectonic zone along the northeastern flank of the Day Nui Con Voi Range in the Red River Shear Zone, in the northern part of Vietnam. Crystals of zircon included in ruby and spinel from Luc Yen and An Phu deposits were dated *in situ* by the U–Pb method with an ion microprobe. The patchy zoning of the zircon crystals and the wide range of ages (266–38 Ma) provide evidence for a complex metamorphic history, with at least two main thermal events: (1) Zircon included in spinel crystals probably crystallized during the Permian (256.6 ± 9.4 Ma), with a possible reopening of their U–Pb system in the early Triassic (231.7 ± 5.6 Ma). (2) Ruby formed at about 38 Ma when the Red River Shear Zone was the site of ductile deformation during the peak of metamorphism. The dating of zircon and phlogopite syngenetic with ruby documents the temporal relationship between high-temperature metamorphism and the cooling history of the Red River metamorphic belt. Ruby deposits hosted by marble sequences in central and southeastern Asia seem to be an excellent marker; they allow an interpretation of the timing of the activity of Cenozoic structures linked to the collision between Indian and Eurasian continents.

Keywords: ruby deposits, marble, zircon, *in situ* U–Pb dating, Cenozoic ages, ion-probe data, electron-microprobe data, cathodoluminescence, northern Vietnam.

§ *E-mail address*: vgarnier@crpg.cnrs-nancy.fr

Sommaire

Des gisements de rubis se rencontrent dans les séquences de marbres de la zone tectonique de Lo Gam située le long du flanc Nord-est de la ceinture métamorphique du Day Nui Con Voi dans la zone de cisaillement du Fleuve Rouge, au Nord du Viêt-nam. Des cristaux de zircon inclus dans un cristal de rubis et dans des cristaux de spinelle issus des gisements de Luc Yen et An Phu on été datés, *in situ*, avec une sonde ionique. Les zonations en taches ainsi que le large intervalle d'âges obtenus (266–38 Ma) témoignent d'une évolution métamorphique complexe, avec au moins deux événements thermiques: (1) les cristaux de zircon inclus dans les cristaux de spinelle ont probablement cristallisé pendant le Permien (256.6 ± 9.4 Ma), et leur système U–Pb probablement été réouvert au début du Trias (231.7 ± 5.6 Ma); (2) le rubis s'est formé vers 38 Ma, pendant le pic du métamorphisme, tandis que la zone de cisaillement du Fleuve Rouge subissait une déformation ductile. La datation des cristaux de zircon et de phlogopite syngénétiques du rubis du Viêt-nam documente les relations temporelles entre le métamorphisme de haute température et le refroidissement de la ceinture métamorphique de la zone de cisaillement du Fleuve Rouge. Les cristaux de rubis associés aux séquences de marbre de l'Asie Centrale et du Sud-est constituent un excellent marqueur temporel qui permet d'analyser l'activité le long de structures tectoniques liées à la collision entre les plaques continentales indienne et eurasienne.

Mots-clés: gisements de rubis, marbre, zircon, datation U–Pb *in situ*, âges cénozoïques, sonde ionique, données de microsonde électronique, cathodoluminescence, Nord du Viêt-nam.

Introduction

The red color of ruby is linked to the replacement of Al by Cr in the crystal structure of corundum. Marble units from central and southeastern Asia are the main source for excellent-quality ruby, with intense color and high transparency. Marble-hosted ruby deposits occur in Tajikistan, Afghanistan, Pakistan, Azad–Kashmir, Nepal, Myanmar, northern Vietnam and southern China (Hughes 1997). Mineralization in marble results from the circulation of fluid and fluid–rock interactions (Giuliani *et al*. 2003), as well as specific tectonic and metamorphic processes related to the formation of thrust and shear zones (Pêcher *et al*. 2002). Marble-hosted ruby deposits from northern Vietnam occur in the Day Nui Con Voi Range (DNCV, Fig. 1A), a metamorphic belt resulting from the continental collision between India and Asia in the Cenozoic (Schärer *et al*. 1990, Leloup *et al*. 1995, Garnier *et al*. 2002).

Dating of phlogopite syngenetic with ruby by the $^{40}Ar/^{39}Ar$ method has yielded Oligocene minimum ages for the deposits located in the Lo Gam tectonic zone (Fig. 1B), on the northeastern flank of the DNCV in the Red River Shear Zone (RRSZ), and Miocene ages for those from the DNCV (Garnier *et al*. 2002). This diachronism led to the hypothesis that ruby formed either in two distinct periods, during the Oligocene in the Lo Gam zone and the Miocene in the DNCV, or in one single period followed by diachronous cooling. To better understand the timing of ruby formation, we undertook the U–Pb dating of zircon included in one crystal of ruby and in several grains of spinel from the Luc Yen and An Phu marble units from the Lo Gam zone with an ion probe. The aim of the present study is to understand how and when ruby hosted in the Lo Gam marble units formed in relation to the collision of the Indian and Eurasian plates.

Geological Setting

The Day Nui Con Voi Range

The Ailao Shan – Red River Shear Zone (ASRR) extends from eastern Tibet to the south China Sea (Fig. 1A) and plays a major role in the strike-slip extrusion of the Indochina block related to the India–Asia collision (Harrison *et al*. 1996). The timing of Tertiary activity along the ASRR has been constrained by more than one hundred $^{40}Ar/^{39}Ar$ ages obtained on metamorphic and plutonic rocks (Harrison *et al*. 1996, Chung *et al*. 1997, Leloup *et al*. 1993, 1995, 2001, Phan Trong *et al*. 1998), indicating that it acted as a sinistral shear-zone from 35 to 17 Ma (Leloup *et al*. 1993, 1995, Schärer *et al*. 1994, Harrison *et al*. 1996) and possibly prior to 36 Ma ago (Leloup *et al*. 2001). According to Lan *et al*. (2001), part of the gneissic belt exposed in the Red River Shear Zone has recorded a mid-Tertiary event (*ca*. 40–25 Ma) corresponding to continental extrusion resulting from the India–Asia collision. The metamorphic and magmatic activity of the Ailao Shan and Diancang Shan areas, which are the northwestern continuation of the DNCV in China, has been studied by U–Pb dating of zircon, monazite, xenotime and titanite from leucogranitic layers and mylonitic gneisses (Schärer *et al*. 1990, 1994, Leloup *et al*. 1993, 1995, 2001, Zhang & Schärer 1999) and by Rb–Sr and K–Ar dating of metamorphic rocks (Tapponnier *et al*. 1990, Leloup *et al*. 2001).

In contrast, there is a lack of similar data for the Day Nui Con Voi Range (DNCV) (Fig. 1). The Red River Shear Zone comprises the DNCV range and, located on the eastern flank of the RRSZ, the Lo Gam tectonic zone. The RRSZ is bounded by two right-lateral strike-slip fault zones, the Song Chay to the northeast and the Red River to the southwest (Fig. 1A). Near the Chinese border, the RRSZ cuts through high-grade

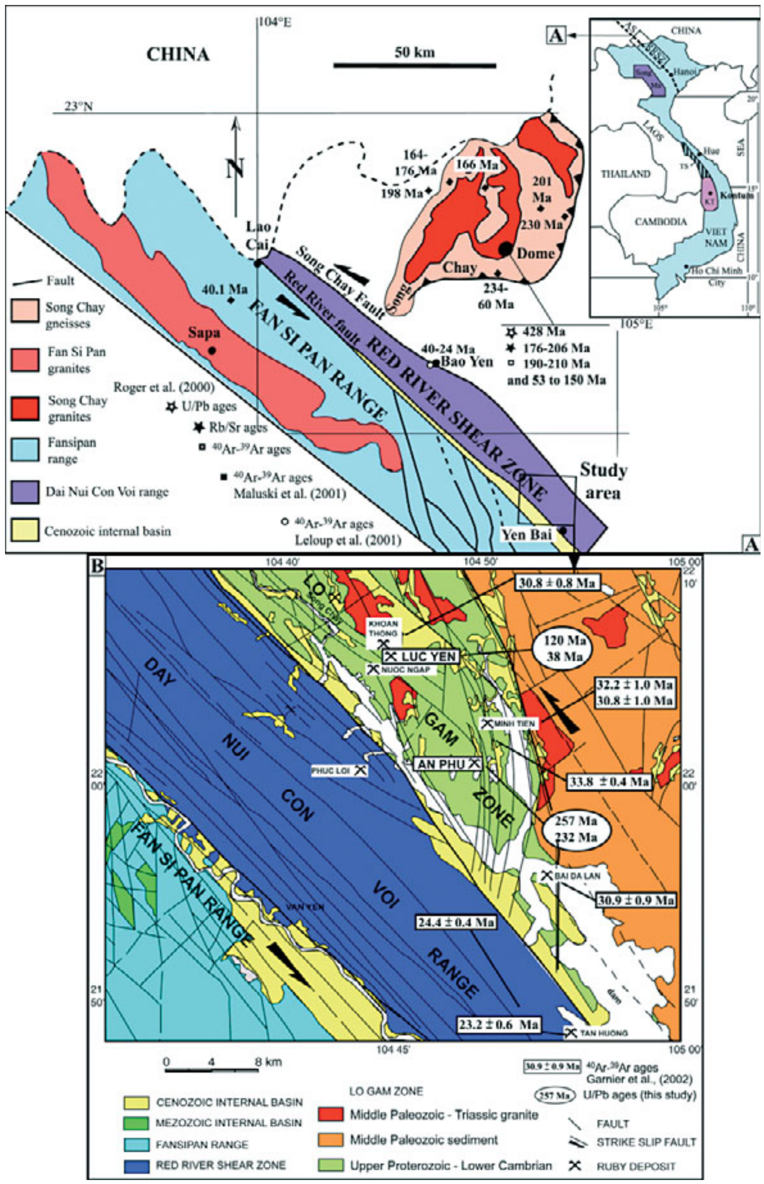

FIG. 1. A. Structural sketch-map of the Red River Shear Zone area, northern Vietnam, modified after Nam *et al*. (1998) and Roger *et al*. (2000). AS–RRSZ: Ailao Shan – Red River Shear Zone, KT: Kontum massif, TS: Truong Son belt. B. Simplified geological map showing the major tectonic domains in the area of the Red River Shear Zone (modified after Phan Trong & Hoàng Quang 1997). The main deposits of ruby in the Day Nui Con Voi Range and in the Lo Gam zone are shown, as well as the ^{40}Ar–^{39}Ar and U–Pb ages.

gneisses forming the DNCV range, which are flanked by marble of upper amphibolite grade (Garnier 2003). The structure in the Lo Gam zone is comparable to that observed within the DNCV metamorphic belt: left-lateral shear planes bound, at a large scale, sigmoidal boudins of metamorphic rocks (Leloup *et al*. 2001). These structures result from the same northwest–southeast left-lateral shear that affected the rocks in the RRSZ from 35 to 17 Ma (Leloup *et al*. 1993, 1995).

Ruby deposits of the Lo Gam zone

The Luc Yen ruby deposits occur in the Lo Gam zone in a thick metasedimentary sequence of Cambrian age, composed of marble and overlying sillimanite – biotite – garnet schist (Fig. 1B). These units, bounded by left-lateral faults, are intruded by granitic rocks and related pegmatites of Triassic age (Phan Trong & Hoàng Quang 1997). They are considered to be Neoproterozoic to Cambrian in age. Ruby occurs (a) as crystals disseminated in marble and associated with phlogopite, magnesian tourmaline, margarite, pyrite, rutile and graphite (Bai Da Lan, An Phu, Nuoc Ngap, Luc Yen and Khoan Thong mines, Fig. 1B); (b) in veinlets, associated with calcite, magnesian tourmaline, pyrite, margarite and phlogopite (An Phu mine), and (c) in fissures, associated with graphite, pyrite, phlogopite and margarite (Bai Da Lan mine). The temperature of the peak of metamorphism ranged between 630 and 745°C (Giuliani *et al.* 1999).

Analytical Methods

Crystals of zircon have been examined by back-scattered electron imaging (BSE) with a Hitachi 2500 scanning electron microscope (SEM), with a Technosyn cold cathodoluminescence and with hot cathodoluminescence on a Philips XL 30 scanning electron microscope. The electron-probe micro-analyses (EPMA) were obtained with a Cameca SX 50 instrument. Operating conditions were: acceleration voltage 20 kV, beam intensity 10 nA, and collection time 10 s for major elements (*i.e.*, Zr and Si) and 30 s for trace elements. We used natural and synthetic standards and the PAP program (Pouchou & Pichoir 1991) for data correction.

The U–Pb analyses were performed using the CRPG–CNRS (Nancy, France) Cameca IMS–1270 ion probe. The analytical procedure was described by Deloule *et al.* (2002). The size of the spots varied between 30 × 40 and 10 × 20 μm. Fragments of the Geostandards zircon 91500 from Ontario (Canada), with an age of 1,062.4 ± 0.4 Ma (Wiedenbeck *et al.* 1995), were mounted with samples and measured every three analyses. The external error from this standard has been propagated onto the samples of unknown ages. The decay constants used to calculate the ages are those from Jaffey *et al.* (1971). Corrections for common lead were calculated at the ^{207}Pb–^{206}Pb measured age using the Stacey & Kramers (1975) model of lead evolution.

Petrography and mineralogy of the ruby-bearing marble of the Lo Gam zone

Petrographic and stable isotopes studies (C, O isotopic composition of carbonates enclosing ruby, O isotopes in corundum and H isotopes in mica grains associated with ruby) indicate that the ruby grew in a closed system buffered by metamorphic fluids released during the metamorphic devolatilization of carbonates, which reacted with evaporites (Garnier 2003, Garnier *et al.* 2005). Fluid-inclusion studies have established the unusual chemical composition of the parent fluids, indicative of an evaporitic contribution (Giuliani *et al.* 2003). Viewed in the context of a petrographic study of the samples, these results indicate conditions of formation of gem-quality ruby during the retrograde path of metamorphism (T in the range 630 to 670°C, P between 2.9 and 3.3 kbar). The aluminum and the chromophores (chromium and vanadium) originate from the marble. The ruby mineralization is restricted to peculiar horizons of impure marble, enriched in detrital minerals (in particular, clay minerals) and in organic matter, and intercalated evaporite layers (salts and sulfate). The S isotope composition of anhydrite and the B isotope composition of tourmaline, both associated with ruby in Vietnam, corroborate the participation of marine and nonmarine evaporites in the formation of ruby, and the deposits of these sediments in a restricted basin enriched in organic matter. All these features lead to the proposal that the marbles protoliths were deposited in an endorheic environment, such as a lagoon (Garnier 2003).

Two peculiar mineralogical associations are of interest in the ruby-bearing marbles from the Lo Gam zone in Vietnam. In a third of the samples studied, ruby is associated with spinel (sample V41a). In the others, it is associated with micas, particularly with phlogopite. Sample V41a is a medium-grained white marble from the Nuoc Ngap mine. It contains an amphibole and spinel–corundum association disseminated in calcite (Tables 1, 2). The calcic amphiboles, magnesiohornblende and pargasite, contain inclusions of pure virtually anorthite ($An_{97.5}$ to $An_{98.6}$, Table 3), diopside and calcite. The contribution of the evaporites to the genesis of ruby in marbles is reflected in the composition of the amphibole, which contains noticeable amounts of Na, Cl and F, and in the very calcic composition of the plagioclase, but both invariably contain notable amounts of Na (Tables 1, 3). Grains of spinel are associated with calcite, pyrite and, in some cases, chlorite (Table 1), nearly pure clinochlore. Some grains of spinel are surrounded by a rim of corundum and dolomite (Fig. 2). These assemblages lead to the proposal that in this sample, like in others from the Lo Gam zone in northern Vietnam, corundum has formed from spinel according to the reaction:

$$MgAl_2O_4 + CaCO_3 + CO_2 \rightarrow CaMg(CO_3)_2 + Al_2O_3$$

$$\text{spinel} + \text{calcite} + CO_2 \rightarrow \text{dolomite} + \text{corundum}$$

In other samples of ruby-bearing marble from the Lo Gam zone, phlogopite forms irregular clots, 1–3 cm in length, containing the ruby crystals. Under the microscope, crystals of ruby show syngenetic phlogopite trapped along growth zones. Phlogopite from the ruby-bearing marble and mica grains from ruby-free marble have been dated by ^{40}Ar–^{39}Ar stepwise-heating technique. Both types of mica yielded ages between 30.8 ± 0.8 Ma and 33.8 ± 0.4 Ma (Garnier *et al*. 2002). Andalusite, anatase, diaspore, phengite, anorthite and zoisite are found as solid inclusions in ruby from Luc Yen and Quy Chau (Pham Van *et al*. 2004).

After careful examination of more than forty samples, two crystals of zircon were found as inclusions in one crystal of ruby from the marble at Luc Yen, and nine crystals of zircon in several grains of spinel from the marble at An Phu, both mines located in the Lo Gam zone.

TABLE 1. REPRESENTATIVE RESULTS OF ELECTRON-MICROPROBE ANALYSES OF AMPHIBOLE AND CHLORITE FROM THE NUOC NGAP MINE

Number	1 Amp	2 Amp	3 Amp	4 Amp	1 Chl	2 Chl
SiO_2 wt.%	50.04	49.70	44.93	44.97	29.86	30.34
TiO_2	0.43	0.32	0.57	0.54	0.11	0.12
Al_2O_3	10.90	10.53	15.23	15.63	24.07	24.54
Cr_2O_3	0.00	0.05	0.01	0.02	0.00	0.01
Fe_2O_3 calc.	0.00	0.00	0.23	0.00		
FeO calc.	0.61	0.80	0.48	0.59	0.12	0.33
MnO	0.00	0.00	0.00	0.04	0.00	0.00
MgO	20.91	20.57	19.36	19.18	32.12	33.82
CaO	13.48	12.59	13.45	13.31	0.02	0.08
Na_2O	1.89	1.55	2.53	2.58	0.01	0.04
K_2O	0.16	0.14	0.44	0.36	0.03	0.00
ZrO	0.00	0.08	0.00	0.00	0.00	0.00
NiO	0.00	0.01	0.00	0.01	0.00	0.00
F	0.38	0.25	0.42	0.40		
Cl	0.02	0.03	0.03	0.04		
H_2O calc.	2.00	2.02	1.93	1.94	12.89	13.28
-O=F	0.16	0.11	0.18	0.17		
-O=Cl	0.00	0.01	0.01	0.01		
Si *apfu*	6.848	6.926	6.289	6.288	5.556	5.478
^{IV}Al	1.152	1.074	1.711	1.712	2.444	2.522
^{VI}Al	0.607	0.655	0.801	0.863	2.835	2.700
Ti	0.044	0.033	0.060	0.057	0.015	0.016
Cr	0.000	0.005	0.001	0.002	0.000	0.001
Fe^{3+}	0.000	0.000	0.024	0.000		
Fe^{2+}	0.070	0.093	0.056	0.069	0.019	0.050
Mn	0.000	0.000	0.000	0.004	0.000	0.000
Mg	4.266	4.274	4.039	3.997	8.910	9.103
Ca	1.977	1.880	2.018	1.993	0.004	0.015
Na	0.502	0.419	0.685	0.699	0.004	0.014
K	0.028	0.025	0.079	0.064	0.007	0.000
Zr	0.000	0.005	0.000	0.000	0.000	0.000
Ni	0.000	0.001	0.000	0.001	0.000	0.000
F	0.164	0.112	0.185	0.178		
Cl	0.005	0.007	0.008	0.009		
OH	1.831	1.881	1.807	1.813	16.000	16.000

The formula of an amphibole is calculated on the basis of 23 atoms of oxygen and 13 cations in the tetrahedrally coordinated and *C* (*M*1, *M*2 and *M*3) sites, according to IMA recommendations (Leake *et al*. 1997, 2003). The amphibole is classified as magnesiohornblende. The structural formula of chlorite is calculated on the basis of 28 atoms of oxygen. The chlorite is classified as clinochlore. These compositions pertain to sample V41a.

Characterization of the Zircon Included in Ruby and Spinel

Morphology

The zircon crystals share common features: (1) a size between 50 and 150 μm long and 50 to 75 μm across; the largest are those included in the ruby from Luc Yen; (2) prismatic shape (length:width ratio < 2), with pyramidal terminations. Cathodoluminescence (CL) images (Fig. 3) of both crystals of zircon included in the ruby show a core surrounded by several overgrowths. Sample LY1 has a bright-CL core surrounded by dark-CL overgrowth, whereas sample LY2 has a CL-free black core surrounded by several lighter-colored growth-zones.

Most of the zircon crystals included in the spinel grains show a complex texture with patchy zoning visible in BSE and CL images (Figs. 4, 5). The zones are commonly light or dark grey on both CL and BSE images, indicating variable amounts of trace elements from one zone to another (bright-CL zones are U-poor, as U suppresses CL, and bright-BSE zones are rich in U, *i.e*., heavy atomic species) with an irregular and, in some cases, an amoeba-like shape. These textures provide evidence for a complex growth-history, but the

TABLE 2. REPRESENTATIVE RESULTS OF ELECTRON-MICROPROBE ANALYSES OF SPINEL AND CORUNDUM FROM THE NUOC NGAP MINE

	Spl	Spl	Crn	Crn
SiO_2 wt.%	0.00	0.00	0.00	0.00
TiO_2	0.02	0.01	0.02	0.03
Al_2O_3	71.11	70.82	99.19	99.23
Cr_2O_3	0.09	0.10	0.14	0.12
Fe_2O_3 calc	0.00	0.00	0.03	0.04
V_2O_3	0.00	0.00	0.01	0.01
FeO calc	0.91	1.00		
MnO	0.00	0.00	0.00	0.00
MgO	27.14	27.30	0.43	0.08
ZnO	0.12	0.06	0.00	0.00
NiO	0.00	0.00		
CoO	0.00	0.00	0.00	0.00
Ga_2O_3			0.01	0.01
Total	99.41	99.28	99.84	99.51
Si *apfu*	0.000	0.000	0.000	0.000
Ti	0.000	0.000	0.000	0.000
Al	2.005	2.000	1.992	1.996
Cr	0.002	0.002	0.002	0.002
Fe^{3+}	0.000	0.000	0.000	0.001
V	0.000	0.000	0.000	0.000
Fe^{2+}	0.018	0.020		
Mn	0.000	0.000	0.000	0.0000
Mg	0.965	0.975	0.008	0.002
Zn	0.002	0.001	0.000	0.000
Ni	0.000	0.000		
Co	0.000	0.000	0.000	0.000
Ga			0.000	0.000
Total	2.996	2.999	2.002	2.000

The structural formula of spinel (Spl) is based on four atoms of oxygen and Fe^{2+}:Fe^{3+} partitioning according to stoichiometry. The structural formula of corundum (Crn) is based on three atoms of oxygen. These compositions pertain to sample V41a.

absence of altered zones and reaction rims in the grains indicates that the zircon was not affected by metamictization, which could have led to volume diffusion of lead (Geisler *et al*. 2002).

Chemical composition in terms of major elements

The EMPA analyses show contrasting chemical compositions among zones. There is small variation of Zr and Si contents among crystals. Only the Hf contents show noticeable variations within single grains. ZrO_2, SiO_2 and HfO_2 contents range respectively between 62.2 and 67.3, 30.6 and 32.9, and 0.8 and 2.0 wt.%. In a single grain, the Hf contents can vary by 50% (anal. LY2–1 and LY2–2, Table 4).

Chemical composition in terms of trace elements

The UO_2 contents are less than 1.2 wt.%; ThO_2 and Y_2O_3 contents are respectively less than or equal to 0.8 and 1.3 wt.% (Figs. 4A, B, Tables 4, 5). The dark grey areas observed on BSE images are generally depleted in these trace elements relative to the light grey areas, as the BSE brightness increases with atomic number (Fig. 4); on the contrary, the dark grey areas observed on CL images are enriched in these elements, as U suppresses CL in zircon (Figs. 3, 5).

In zircon included in the ruby from Luc Yen, Si virtually fills the *Si* site, and Hf substitutes to a slight extent for Zr, from 0.009 to 0.018 *apfu*. Thorium, U, REE and Y are below the detection limit of the electron microprobe. The zircon crystals included in the spinel from An Phu, Zr is replaced by between 0.007 and 0.023 *apfu* Hf. The other trace elements are close to the detection limit of the electron microprobe; some exceptional values of Th, U and especially Y reach up to 0.008, 0.006, and 0.022 *apfu*, respectively. The Th and Y contents of zircon are positively correlated with U contents (Table 5, Fig. 6). Zircon crystals included in the spinel grains are all richer in U, Th and Y than those included in the ruby crystal (Table 5, Fig. 6).

U–Pb Ages of the Crystals

Zircon crystals included in the ruby

Three analyses were made in each of the zircon crystals LY–1 and LY–2, in distinct zones (Fig. 3). These crystals yielded, respectively, $^{238}U–^{206}Pb$ ages between 192.5 ± 9.4 Ma and 38.1 ± 2.0 Ma, and between 119.7 ± 2.0 Ma and 54.2 ± 1.6 Ma (Table 6, Fig. 3). They have very low Pb contents with a relatively high proportion of common Pb (2.2 to 18%, Fig. 7A). The correction for common lead has an important impact on young ages; as a consequence, the $^{207}Pb–^{206}Pb$ ages cannot be calculated precisely. Only the corrected $^{238}U–^{206}Pb$ ages will be considered here. As shown in Table 6, the $^{207}Pb–^{206}Pb$ ages, as well as the $^{235}U–^{207}Pb$ ages, are poorly defined, with large errors where the Pb contents are below 1 ppm.

The $^{238}U–^{206}Pb$ age of 45.1 ± 1.6 Ma measured in sample LY–1 represents a mixed age, as it was not

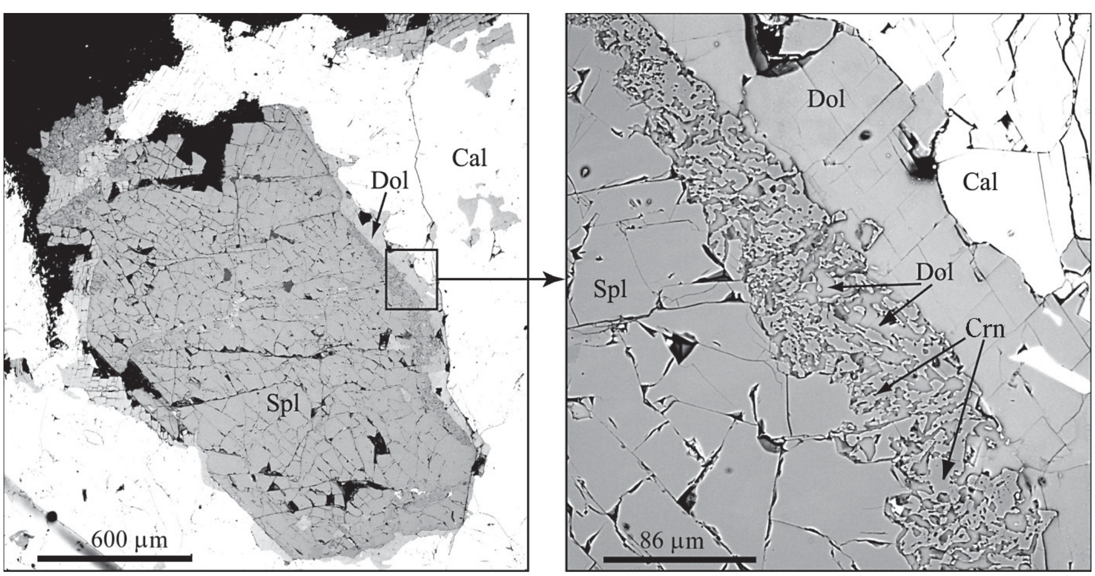

FIG. 2. Spinel–corundum association found in sample V41a from Nuoc Ngap mine (BSE images). Dol: dolomite, Cal: calcite, Spl: spinel, Cor: corundum.

recorded from a single growth-zone, in contrast to the age of 38.1 ± 2.0 Ma that was measured in the outer rim of this crystal (Fig. 3A). The growth-zones are not well defined in every case on CL images, and it appears from Figure 3A that the ^{238}U–^{206}Pb age of 192.5 ± 9.4 Ma may have been obtained from a single growth-zone. In this case, this age may be of geological significance, providing that the crystal did not lose Pb after its crystallization. If this age was obtained from several growth-zones, it then represents a minimum age for the crystallization of the core of the zircon crystal.

The ^{207}Pb–^{206}Pb ages corresponding to the ^{238}U–^{206}Pb ages of 119.7 ± 2.0 Ma and 38.1 ± 0.5 Ma are poorly defined, as the corresponding common lead contents are high (Fig. 7A). However, the data presented in Table 6 highlight the fact that even if the errors are important for ^{235}U–^{207}Pb ages corresponding to the ^{238}U–^{206}Pb ages of 119.7 ± 2.0 Ma and 38.1 ± 0.5 Ma, these ages are concordant within the analytical uncertainties and must reflect "true" ages. The ^{238}U–^{206}Pb ages of 109.3 ± 3.7 Ma and 54.2 ± 1.6 Ma measured for sample LY–2 also represent mixed ages; however, the oldest age of this sample, 119.7 ± 2.0 Ma, entirely recorded in the core, may represent the age of crystallization of this core if this crystal suffered no lead loss. If true, this age corresponds to a minimum age for zircon crystallization. Moreover, the growth zones surrounding the core of this sample must be younger than 54 Ma, which is a mixed age between the lighter overgrowth seen on the CL image (Fig. 3B) and the core. These ^{238}U–^{206}Pb ages are consistent with the growth zoning observed on CL images (Figs. 3A, B). They show evidence that: 1) these crystals contain an inherited core. In sample LY–1, the core may have crystallized at 193 Ma, but possibly before, as explained above; in sample LY–2, the core probably crystallized at about 120 Ma. 2) The outer rim of sample LY–1 crystallized at about 38 Ma; the growth zones of sample LY–2, surrounding the core, must be younger than 54 Ma. Note that the overgrowth on the core of these crystals may

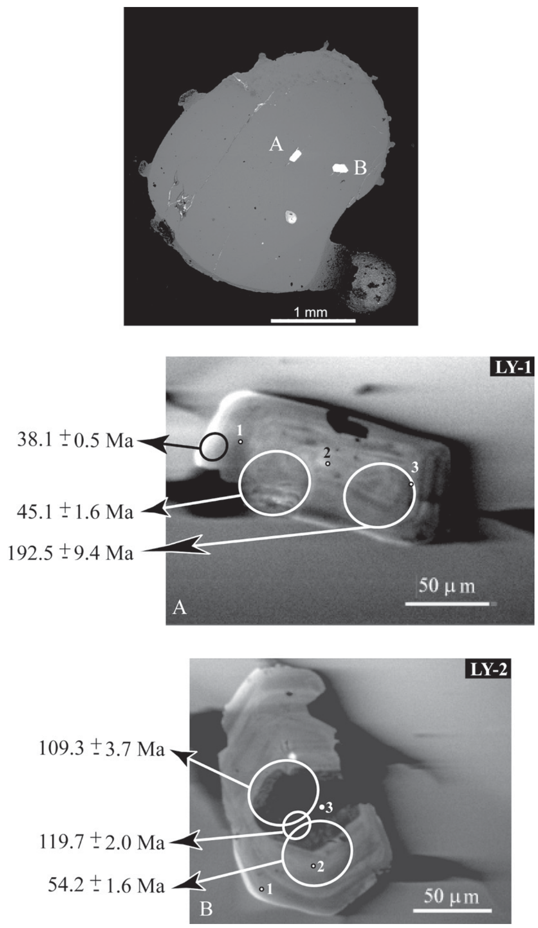

FIG. 3. (Above) Back-scattered electron image of the ruby crystal with two included zircon crystals (marked A and B); (A, B) CL images of both zircon crystals included in the ruby grain. Numbered dots locate the sites of EPMA analyses, with results reported in Table 4; white ellipses correspond to the analytical ion-microprobe spots, and the related ^{206}Pb–^{238}U ages are specified.

TABLE 3. REPRESENTATIVE RESULTS OF ELECTRON-MICROPROBE ANALYSES OF FELDSPAR FROM NUOC NGAP MINE

SiO_2 wt.%	43.07	43.43	43.64	43.26
TiO_2	0.00	0.00	0.00	0.01
Al_2O_3	36.34	36.18	36.49	36.24
Fe_2O_3	0.06	0.00	0.06	0.07
MnO	0.00	0.05	0.00	0.00
MgO	0.00	0.06	0.03	0.07
CaO	20.48	20.04	20.21	20.29
SrO	0.00	0.00	0.00	0.00
BaO	0.00	0.00	0.00	0.00
Na_2O	0.16	0.29	0.26	0.20
K_2O	0.00	0.00	0.00	0.01
Rb_2O	0.00	0.00	0.00	0.00
Total	100.10	100.05	100.68	100.15
Si *apfu*	1.997	2.012	2.009	2.004
Ti	0.000	0.000	0.000	0.000
Al	1.986	1.975	1.980	1.978
Fe^{3+}	0.002	0.000	0.002	0.002
Mn	0.000	0.002	0.000	0.000
Mg	0.000	0.004	0.002	0.005
Ca	1.018	0.995	0.997	1.007
Sr	0.000	0.000	0.000	0.000
Ba	0.000	0.000	0.000	0.000
Na	0.015	0.026	0.023	0.018
K	0.000	0.000	0.000	0.000
Rb	0.000	0.000	0.000	0.000
Total	5.017	5.014	5.012	5.014
Ab mol.%	1.42	2.54	2.30	1.71
An	98.58	97.46	97.70	98.26
Or	0.000	0.000	0.000	0.003

The structural formula of feldspar, anorthite in each case, is calculated on the basis of eight atoms of oxygen.

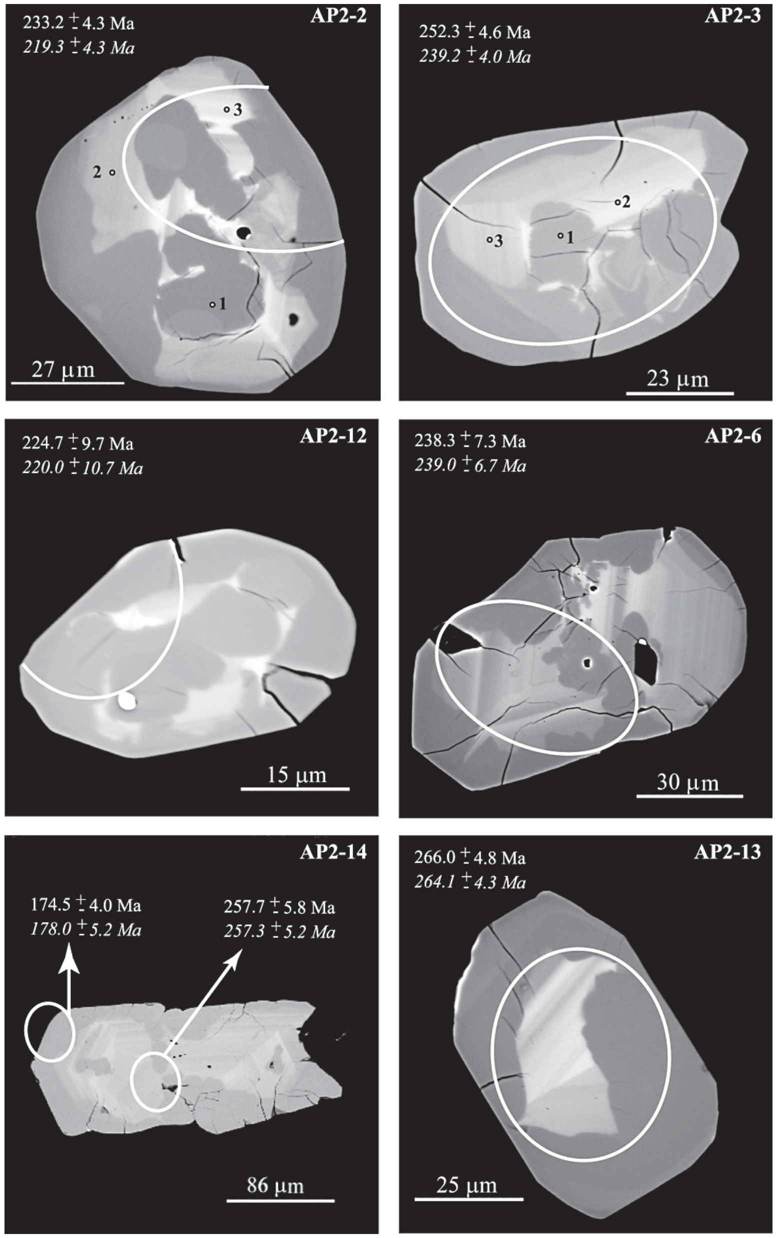

FIG. 4. Back-scattered SEM images of six of the zircon crystals included in spinel grains. Numbered dots locate the EPMA analyses reported in Table 5; white ellipses correspond to the analytical ion-probe spots, and the related $^{238}U–^{206}Pb$ ages are specified.

have grown during one or several events. The youngest episode of growth recorded in these crystals has an age of about 38 Ma.

Zircon crystals included in spinel

Ten U–Pb analyses were made on zircon included in spinel (Table 6). Most of these zircon crystals are very small, seven of them averaging less than 60 μm across (Figs. 4, 5). Thus, only one or rarely two analyses per crystal could be performed. There is considerable chemical variation within the crystals (Table 5, Figs. 4, 5), and each spot analyzed overlaps several zones. These zircon crystals also show an enrichment in common lead (Fig. 7B). The $^{238}U–^{206}Pb$ ages range between 174.4 ± 4.0 Ma and 266.0 ± 4.7 Ma (Table 6). Five of the ten sets of $^{207}Pb–^{206}Pb$ and $^{235}U–^{207}Pb$ ages are concordant within the analytical uncertainties, and eight of the ten $^{238}U–^{206}Pb$ and $^{235}U–^{207}Pb$ ages are concordant within the analytical uncertainties. The $^{207}Pb–^{206}Pb$ ages are very sensitive to the common lead correction, explaining the large scatter in these ages. The ages recorded in any sample require cautious interpretation, as the analytical spots overlap several chemical zones, and as Pb losses possibly occurred after the crystallization of the zircon crystals.

Nine of the ten $^{238}U–^{206}Pb$ measured ages have a bimodal distribution with peaks at 231.7 ± 5.6 Ma and 256.6 ± 9.4 Ma; the regression through the points corresponding to these nine ages in a Tera–Wasserburg diagram yield an intercept age of 235 ± 19 Ma. Owing to the small dataset, and lacking other evidence, it is not possible to assign these peaks to two distinct events. This result suggests that the protolith of the zircon crystals has recorded two successive events: the first one at about 257 Ma, and the second one at about 232 Ma. But it may be possible to explain this distribution by a random loss of lead. However, the three U–Pb ages corresponding to the $^{238}U–^{206}Pb$ ages of 228.1 ± 5.2, 238.3 ± 7.3 and 257.7 ± 5.8 Ma are respectively concordant. This leads to the proposal that the peak at 257 Ma could represent the age of zircon crystallization, during the early Permian, and the peak at 232 Ma could correspond to a reopening of the U/Pb system in the early Triassic (Fig. 8). But owing to the small dataset, this is a non-unique interpretation. The lead loss may have occurred more recently, leading to a similar distribution of the ages.

A single younger age was measured, 174.4 ± 4.0 Ma (Table 6, Fig. 8). This dataset, yielding an age of 174.4 ± 4.0 Ma, must have recorded recent loss in lead, as shown by the Tera–Wasserburg concordia (Fig. 7B).

TABLE 4. REPRESENTATIVE RESULTS OF ELECTRON-MICROPROBE ANALYSES OF ZIRCON CRYSTALS INCLUDED IN A GRAIN OF RUBY FROM THE LUC YEN MINE

	Zrn 1	Zrn 2	Zrn 3	Zrn 4	Zrn 5	Zrn 6
P_2O_5 wt.%	0.00	0.00	0.00	0.000	0.00	0.03
SiO_2	32.57	32.14	32.59	32.12	32.48	32.22
TiO_2	0.00	0.00	0.00	0.00	0.00	0.00
ZrO_2	66.24	65.91	66.38	65.74	65.48	63.88
HfO_2	1.21	1.25	1.11	0.99	1.10	2.04
UO_2	b.d.l.	b.d.l.	b.d.l.	b.d.l.	b.d.l.	b.d.l.
ThO_2	b.d.l.	b.d.l.	b.d.l.	b.d.l.	b.d.l.	b.d.l.
Al_2O_3	b.d.l.	b.d.l.	b.d.l.	0.02	b.d.l.	0.03
Y_2O_3	b.d.l.	b.d.l.	b.d.l.	b.d.l.	b.d.l.	b.d.l.
Tb_2O_3	b.d.l.	b.d.l.	b.d.l.	b.d.l.	b.d.l.	b.d.l.
Dy_2O_3	b.d.l.	b.d.l.	b.d.l.	b.d.l.	b.d.l.	b.d.l.
FeO	b.d.l.	b.d.l.	b.d.l.	b.d.l.	b.d.l.	0.19
PbO	b.d.l.	0.04	b.d.l.	b.d.l.	b.d.l.	b.d.l.
Total	100.02	99.34	100.08	98.87	99.06	98.39
P *apfu*	0.000	0.000	0.000	0.000	0.000	0.001
Si	0.999	0.994	0.998	0.996	1.003	1.005
Ti	0.000	0.000	0.000	0.000	0.000	0.000
Zr	0.990	0.994	0.991	0.994	0.986	0.972
Hf	0.011	0.011	0.010	0.009	0.010	0.018
U	b.d.l.	b.d.l.	b.d.l.	b.d.l.	b.d.l.	b.d.l.
Th	b.d.l.	b.d.l.	b.d.l.	b.d.l.	b.d.l.	b.d.l.
Al	b.d.l.	b.d.l.	b.d.l.	0.001	b.d.l.	0.001
Y	b.d.l.	b.d.l.	b.d.l.	b.d.l.	b.d.l.	b.d.l.
Tb	b.d.l.	b.d.l.	b.d.l.	b.d.l.	b.d.l.	b.d.l.
Dy	b.d.l.	b.d.l.	b.d.l.	b.d.l.	b.d.l.	b.d.l.
Fe	b.d.l.	b.d.l.	b.d.l.	b.d.l.	b.d.l.	0.005
Pb	b.d.l.	0.000	b.d.l.	b.d.l.	b.d.l.	b.d.l.
Total	2.000	1.999	1.999	2.000	1.999	2.002

The structural formula of zircon (Zrn) is calculated on the basis of four atoms of oxygen. b.d.l.: below detection limit.

TABLE 5. REPRESENTATIVE RESULTS OF ELECTRON-MICROPROBE ANALYSES OF ZIRCON CRYSTALS INCLUDED IN GRAINS OF SPINEL FROM THE AN PHU MINE

	Zrn 1	Zrn 2	Zrn 3	Zrn 4	Zrn 5	Zrn 6
P_2O_5 wt.%	0.00	0.17	0.34	0.00	0.40	0.06
SiO_2	32.54	32.86	32.32	32.54	31.82	32.58
TiO_2	0.00	0.00	0.00	0.00	0.00	0.00
ZrO_2	67.32	65.59	64.88	65.94	64.83	65.45
HfO_2	0.85	1.25	1.19	1.47	1.09	1.29
UO_2	0.07	0.29	0.67	0.10	0.85	0.42
ThO_2	0.05	0.08	0.27	b.d.l.	0.35	0.14
Al_2O_3	0.00	0.01	0.00	0.00	0.00	0.00
Y_2O_3	b.d.l.	0.32	0.68	0.05	0.79	0.29
Tb_2O_3	b.d.l.	b.d.l.	b.d.l.	b.d.l.	b.d.l.	b.d.l.
Dy_2O_3	b.d.l.	0.05	0.05	0.04	0.05	b.d.l.
FeO	b.d.l.	b.d.l.	0.05	b.d.l.	b.d.l.	0.05
PbO	b.d.l.	b.d.l.	b.d.l.	b.d.l.	b.d.l.	b.d.l.
Total	100.83	100.62	100.45	100.14	100.18	100.28
P *apfu*	0.000	0.004	0.009	0.000	0.011	0.002
Si	0.991	1.001	0.992	0.998	0.983	1.000
Ti	0.000	0.000	0.000	0.000	0.000	0.000
Zr	1.000	0.975	0.971	0.987	0.976	0.979
Hf	0.007	0.011	0.010	0.013	0.010	0.011
U	0.000	0.002	0.005	0.001	0.006	0.003
Th	0.000	0.001	0.002	b.d.l.	0.002	0.001
Al	0.000	0.000	0.000	0.000	0.000	0.000
Y	b.d.l.	0.005	0.011	0.001	0.013	0.005
Tb	b.d.l.	b.d.l.	b.d.l.	b.d.l.	b.d.l.	b.d.l.
Dy	b.d.l.	0.000	0.000	0.000	0.000	b.d.l.
Fe	b.d.l.	b.d.l.	0.001	b.d.l.	b.d.l.	0.001
Pb	b.d.l.	b.d.l.	b.d.l.	b.d.l.	b.d.l.	b.d.l.
Total	1.998	1.999	2.001	2.000	2.001	2.002

The structural formula of zircon (Zrn) is calculated on the basis of four atoms of oxygen. b.d.l.: below detection limit.

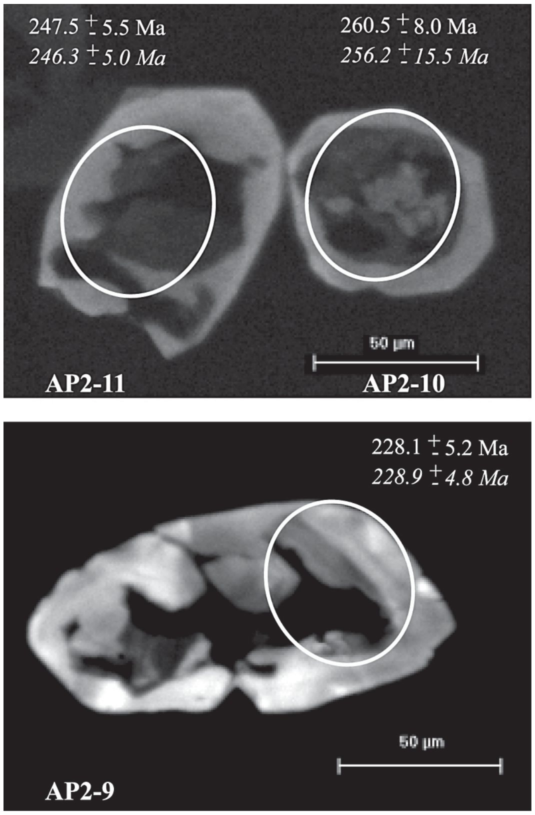

FIG. 5. CL images of three other zircon crystals included in spinel. White ellipses correspond to the analytical ion-microprobe spots, and the related $^{238}U–^{206}Pb$ ages are specified.

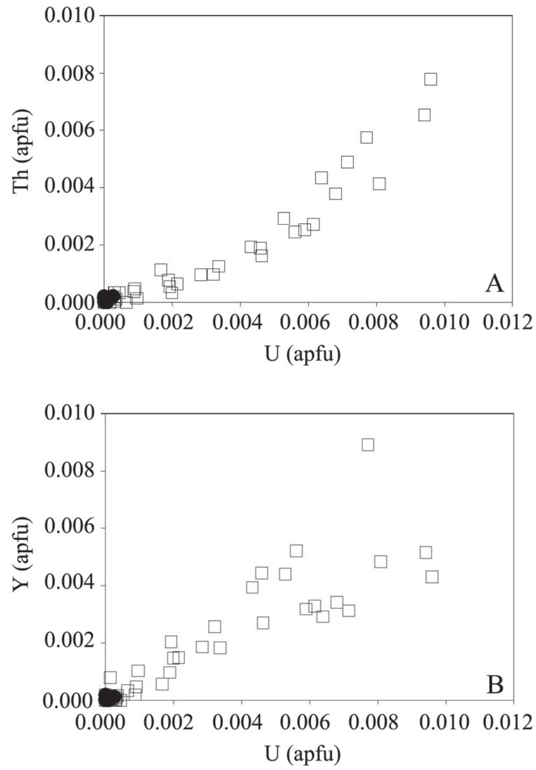

FIG. 6. Concentrations (in *apfu*) of (A) Th *versus* U, and (B) Y *versus* U in zircon crystals; black dots: zircon crystals included in the ruby grain, open squares: zircon crystals included in the spinel grains.

DISCUSSION: ZIRCON CRYSTALS INCLUDED IN RUBY AND SPINEL BEAR WITNESS OF THE TECTONOMETAMORPHIC EVOLUTION OF THE RED RIVER SHEAR ZONE

The U–Pb dating of zircon crystals included in spinel and ruby provides evidence for a complex metamorphic history of the Lo Gam zone, with two high-temperature thermal events, the first in the Permian at 257 Ma, and the second in the Eocene at 38 Ma.

Zircon crystals in ruby

These zircon crystals, found as solid inclusions arranged along growth zones of the ruby, are associated with primary fluid inclusions (Giuliani *et al*. 2003). They may represent either syngenetic solids trapped during the growth of the host or xenocrysts carried by the parent fluid of the ruby. The high-temperature conditions for ruby formation, up to 670°C (Giuliani *et al*. 1999), suggest that these overgrowth zones in zircon formed during the latest stage of ruby crystallization. As a result, the $^{238}U–^{206}Pb$ age of 38.1 ± 0.5 Ma indicates that ruby formed at the Eocene–Oligocene boundary, at which time ductile deformation was active in the Ailao Shan – Red River Shear Zone. The older ages indicate that the zircon cores are xenocrystic.

The $^{40}Ar–^{39}Ar$ dating of micas syngenetic with the ruby yielded Oligocene cooling ages, between 30.8 and 34 Ma, indicating that ductile deformation ceased in the Oligocene in the Lo Gam zone and was followed by rapid cooling of the marble (Garnier *et al*. 2002). The $^{238}U–^{206}Pb$ age of 38.1 ± 2.0 Ma found is in agreement with those younger cooling ages and with the assertion of Leloup *et al*. (2001) that the Ailao Shan – Red River Shear Zone was active between 35 and 17 Ma, and possibly prior to 36 Ma.

The $^{238}U–^{206}Pb$ age of 192.5 ± 9.4 Ma is close to the Rb–Sr age of 206 ± 10 Ma and the $^{40}Ar–^{39}Ar$ ages of 209 ± 9 Ma and 190 ± 8 Ma recorded from the Song Chay Massif (Fig. 1A). This correspondence allows us to propose that this age is of geological significance (see discussion in the previous section). These ages are interpreted to result from a late Triassic event followed by a rapid cooling until the early Jurassic (Leloup *et al*. 1999, Maluski *et al*. 1999, Roger *et al*. 2000). Thus we may infer that this Triassic event has also been recorded in the Lo Gam zone.

Zircon crystals in spinel

Despite the peak at 232 Ma indicating early Triassic reopening of the U–Pb system, the 257–232 Ma ^{238}U–^{206}Pb age range found in zircon crystals from the RRSZ overlaps the 240–245 Ma age range already measured on syn- to late-kinematic micas by ^{40}Ar–^{39}Ar in the Song Ma mafic–ultramafic complex, in the Truong Son belt and in the Kontum Massif (Fig. 1). These ages are interpreted as supporting evidence for the influence of Triassic metamorphism in Vietnam (Maluski *et al*. 2001; Fig. 1A), as has already been found in the south of China and in Thailand (Leloup *et al*. 2001 , Maluski *et al*. 2001). Furthermore, U–Pb ages ranging from 258 ± 6 Ma and 243 ± 5 Ma have been recorded by zircon crystals from gneisses, migmatites and charnockites from the Kontum Massif in central Vietnam, the Bu Khang Dome in north-central Vietnam, and Van Ban in the pre-Mesozoic metamorphic belt located on the western edge of the Day Nui Con Voi (Carter *et al*. 2001). Carter *et al*. (2001) concluded that a large part of the continental crust was affected by a short-lived episode of ductile deformation and high-temperature metamorphism between 258 ± 6 Ma and 243 ± 5 Ma. The U–Pb ages of the present study are in agreement with this conclusion.

The recognition of a *ca*. 280–240 Ma magmatic arc along the northern margin of the Indochina block and a *ca*. 240 Ma metamorphic belt in the Song Ma area, northern Vietnam, suggests that the collision of Indochina with southern China occurred in the Early Triassic (Lepvrier *et al*. 1997, Chung *et al*. 1999, Lan *et al*. 2000, 2001). This event corresponds to the Indosinian orogeny (Lan *et al*., 2001). Li *et al*. (1993) proposed also that the collision between the North China and the Yangtse blocks began in the late Permian or early Triassic, with north-dipping subduction, followed by subduction of the continental crust of the Yangtse block under the North China block during the Triassic. The ^{238}U–^{206}Pb

TABLE 6. U–Pb ISOTOPIC DATA FOR ZIRCON CRYSTALS INCLUDED IN SPINEL FROM THE AN PHU MINE AND IN A GRAIN OF RUBY FROM THE LUC YEN MINE

Measured		Concentrations in ppm			Corrected* and uncorrected ^{238}U/^{206}Pb and ^{207}Pb/^{206}Pb¶				Concordia ages§ in Ma		Ages in Ma					
Analysis	^{206}Pb/^{204}Pb	Pb	U	Th	^{207}Pb/^{206}Pb	σ	^{238}U/^{206}Pb	σ	intercept age	σ	^{206}Pb/^{238}U	σ	^{207}Pb/^{235}U	σ	^{207}Pb/^{206}Pb	σ
Zircon crystals included in spinel crystals, An Phu mine																
AP2-2	2763	71	2244	747	0.05250	0.00045	27.09	0.59	233.3	9.9	233.2	4.3	219.3	4.3	72.9	27.9
AP2-3	3205	105	3056	1266	0.05240	0.00014	26.94	0.59	234.6	9.9	252.3	4.6	239.2	4.0	112.1	8.7
AP2-6	49344	114	3534	1605	0.05124	0.00017	26.55	0.59	238.0	10.0	238.3	7.3	239.0	6.7	245.7	7.7
AP2-9	54463	140	4509	2002	0.05105	0.00010	27.76	0.61	228.1	9.7	228.1	5.2	228.9	4.8	237.2	5.1
AP2-10	882	99	2806	1578	0.06699	0.00160	23.76	0.53	262.0	11.0	260.5	8.0	256.2	15.5	217.3	136.5
AP2-11	24255	114	3399	1731	0.05135	0.00008	25.53	0.56	248.0	10.0	247.5	5.5	246.3	5.0	234.9	4.3
AP2-12	1487	45	1491	589	0.05823	0.00101	32.27	0.73	195.1	8.9	224.7	9.7	220.0	10.7	169.3	72.3
AP2-13	128228	114	3138	1398	0.05112	0.00009	25.09	0.55	252.0	11.0	266.0	4.7	264.1	4.3	247.6	4.4
AP2-14.1	11263	13	545	143	0.05165	0.00023	36.84	0.81	172.3	7.3	174.4	4.0	178.0	4.0	255.0	14.3
AP2-14.2	166052	104	2957	1065	0.05131	0.00005	24.23	0.53	261.0	11.0	257.7	5.8	257.3	5.2	254.5	2.6
Zircon crystal included in a crystal of ruby, Minh Tien mine																
LY-1.1	226	0.4	73	10	0.05027	0.00116	132.19	3.46	48.4	2.5	45.1	1.6	-	-	0.0	0.0
LY-1.2	233	0.5	20	9	0.05794	0.00314	31.29	0.82	201.0	10.0	192.5	9.4	63.1	38.7	0.0	0.0
LY-1.3	94	0.8	161	10	0.21110	0.00257	136.14	1.34	39.1	0.8	38.1	0.5	50.1	11.3	668.6	430.6
LY-2.1	695	0.9	128	20	0.04979	0.00074	115.80	3.03	55.3	2.8	54.2	1.6	37.7	3.0	0.0	0.0
LY-2.2	347	8.3	566	194	0.08907	0.00290	55.41	1.45	110.4	5.7	109.2	3.7	107.1	10.1	58.8	210.5
LY-2.3	752	10.3	638	265	0.07281	0.00349	52.07	0.51	119.5	2.5	119.7	2.0	131.7	10.0	354.9	171.0

* Correction includes the analytical statistical error, the error associated with common lead correction, and the systematic error associated with the U/Pb calibration procedure.

§ Age obtained on the inverse Concordia after regression corresponding to the correction for common lead. ¶ Tera-Wasserburg diagram.

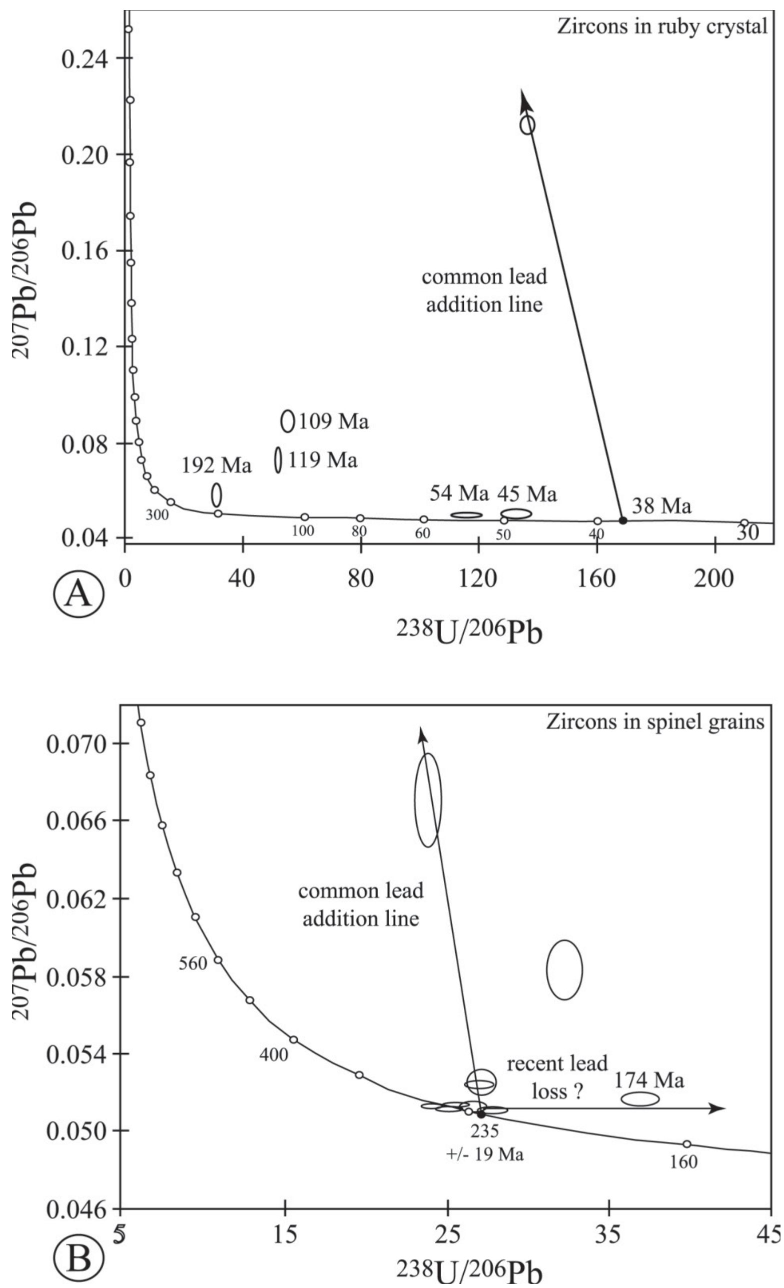

FIG. 7. Tera–Wasserburg concordia diagram showing enrichment of the samples in common lead. (A) Zircon crystals included in the ruby grain. (B) Zircon crystals included in the spinel grains. Data-point error ellipses indicate 68.3% confidence.

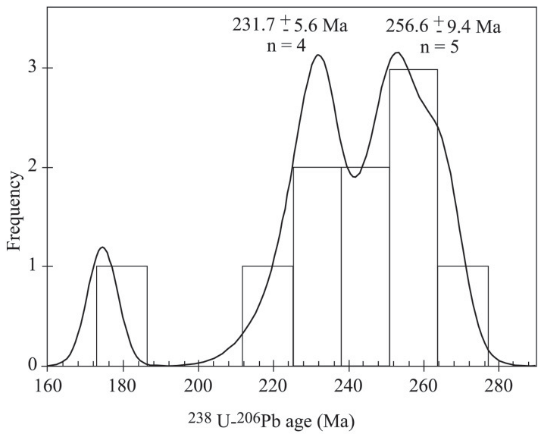

FIG. 8. Histogram of $^{238}U–^{206}Pb$ ages corresponding to the zircon crystals included in spinel grains from the An Phu mine. The value indicated for each mode is the calculated mean value of the corresponding measured $^{238}U–^{206}Pb$ ages (95% confidence).

ages documented in the zircon crystals included in spinel grains from the marble provide evidence for two metamorphic events in the RRSZ, in the Permian and in the Triassic, contemporaneous with the collision of the North China and the Yangtze blocks on one hand, and the collision between the Indochina and the south China blocks on the other.

The U–Pb ages recorded by zircon crystals included in the spinel grains correspond to tectonometamorphic events older than those recorded by zircon crystals included in the ruby. This is in good agreement with the textural observations highlighting the formation of ruby from spinel in the marble units from the Lo Gam zone in Eocene time.

Concluding Remarks

Ruby deposits provide a good marker of the timing of the development of the Red River Shear Zone. Dating by the U–Pb method and $^{40}Ar/^{39}Ar$ dating of phlogopite, minerals syngenetic with ruby, constrain the temporal relationship between the high-temperature metamorphism and the cooling of the ruby-bearing formations. In the Red River Shear Zone, ruby formed around 38 Ma, at temperatures around 650°C. This was followed by diachronous cooling, in the Oligocene in the Lo Gam zone and in the Eocene in the Day Nui Con Voi Range (Garnier *et al.* 2002). This study of ruby deposits reveals the complex metamorphic history of the Lo Gam zone along the northern flank of the Day Nui Con Voi range. The Tertiary activity of the RRSZ has not erased the older tectonometamorphic events recorded in the zircon.

Four fundamental results arise from this study: (1) *in situ* U–Pb dating of syngenetic zircon indicates that ruby formed at about 38 Ma in the Red River Shear Zone, during ductile flow accompanying the peak metamorphism of the Indochina block prior to uplift related to the Himalayan orogeny. (2) Two distinct tectonometamorphic events possibly occurred successively before the Tertiary, at about 257 Ma in the Permian and at 232 Ma in the Early Triassic. (3) Ruby deposits, or more specifically zircon and phlogopite crystals syngenetic with the ruby, seem to be excellent markers for a study of the timing of high-temperature events and cooling histories in shear zones related to the India–Eurasia collision zone. (4) The U–Pb method of *in situ* dating allowed us to decipher the timing of several successive events that occurred in central and southeastern Asia before and during the Himalayan orogeny.

Acknowledgements

This study was supported by Institut pour la Recherche et le Développement, Centre National de la Recherche Scientifique (Centre de Recherches Pétrographiques et Géochimiques), the Programmes Internationaux de Coopération Scientifique (CNRS – Institut National des Sciences de l'Univers and Centre for Natural Sciences and Technology) program. We thank S. Barda, F. Diot and A. Kohler (University Henri Poincaré, Nancy) for SEM images and electron-microprobe data, M. Champenois and D. Mangin (CRPG) for their help in using the ion probe, Dr. P.H. Leloup (Univ. de Lyon) for improving the manuscript and Dr L. Reisberg (CRPG) for carefully correcting the English. We acknowledge the assistance of the Vietnamese Basic Research Program on the Geodynamics of the Red River fault zone. We are grateful to A.M. Cade of the University of British Columbia, Dr. M. Whitehouse of the Swedish Museum of Natural History and Robert F. Martin for their interesting comments that greatly improved the quality of the manuscript.

References

CARTER, A., ROQUES, D., BRISTOW, C. & KINNY, P. (2001): Understanding Mesozoic accretion in southeast Asia: significance of Triassic thermotectonism (Indosinian orogeny) in Vietnam. *Geology* **29**, 211-214.

CHUNG, SUN-LIN, LEE, TUNG-YI, LO, CHING-HUA, WANG, PEI-LING, CHEN, CHIN-YU, NGUYEN TRONG, YEM, TRAN TRONG, HOA & GENYAO, WU (1997): Intraplate extension prior to continental extrusion along the Ailao Shan – Red River shear zone. *Geology* **25**, 311-314.

________, LO, CHING-HUA, LAN, CHING-YING, WANG, PEI-LING, LEE, TUNG-YI, HOA, TRAN TRONG, THAN, HOANG HUU & ANH, TUAN (1999): Collision between Indochina and South China blocks in the Early Triassic: implications for the Indosinian orogeny and closure of eastern-Paleo-Tethys. *Trans. Am. Geophys. Union* (*Eos*) **80**, F1043 (abstr.).

DELOULE, E., ALEXANDROV, P., CHEILLETZ, A., LAUMONIER, B. & BARBEY, P. (2002): In-situ U–Pb zircon ages for Early Ordovician magmatism in the eastern Pyrenees, France: the Canigou orthogneisses. *Int. J. Earth Sci.* **91**, 398-405.

GARNIER, V. (2003): *Les gisements de rubis associés aux marbres de l'Asie Centrale et du Sud-est: genèse et caractérisation isotopique*. Thèse de doctorat, Institut National Polytechnique de Lorraine, Nancy, France.

________, GIULIANI, G., MALUSKI, H., OHNENSTETTER, D., PHAN TRONG, TRINH, HOÀNG QUANG, VINH, PHAM VAN, LONG, VU VAN, TICH & SCHWARZ, D. (2002): Ar–Ar ages in phlogopites from marble-hosted ruby deposits in northern Vietnam: evidence for Cenozoic ruby formation. *Chem. Geol.* **188**, 33-49.

________, ________, OHNENSTETTER D., KAUSAR, A., HOÀNG QUANG, V., PHAN TRONG, T. & PHAM VAN, L. (2005): Les gisements de rubis du Pakistan et du Viêt-nam. *Association Française de Gemmologie* **151**, 6-12.

GEISLER, T., PIDGEON, R.T., VAN BRONSWIJK, W. & KURTZ, R. (2002): Transport of uranium, thorium, and lead in metamict zircon under low-temperature hydrothermal conditions. *Chem. Geol.* **191**, 141-154.

GIULIANI, G., DUBESSY, J., BANKS, D., HOÀNG QUANG, VINH, LHOMME, T., PIRONON, J., GARNIER, V., PHAN TRONG, TRINH, PHAM VAN, LONG, OHNENSTETTER, D. & SCHWARZ, D. (2003): CO_2–H_2S–COS–S_8–AlO(OH)-bearing fluid inclusions in ruby from marble-hosted deposits in Luc Yen area, north Vietnam. *Chem. Geol.* **194**, 167-185.

________, HOÀNG QUANG, V., PHAN TRONG, T., FRANCE-LANORD, C. & COGET, P. (1999): Carbon isotopes study on graphite and coexisting calcite–graphite pairs in marbles from the Luc Yen and Yen Bai districts, north of Vietnam. *Bull. Liaison, Soc. Fr.Minéral.Cristallogr.* **11**, 80-82.

HARRISON, T.M., LELOUP, P.H., RYERSON, F.J., TAPPONNIER, P., LACASSIN, R. & CHEN, W. (1996): Diachronous initiation of transtension along the Ailao Shan – Red River shear zone, Yunnan and Vietnam. *In* The Tectonic Evolution of Asia (A. Yin & T.M. Harrison, eds.). Cambridge University Press, New York, N.Y. (205-226).

HUGHES, R.W. (1997): *Ruby and Sapphire*. RW Hughes Publishing, Boulder, Colorado.

JAFFEY, A.H., FLYNN, K.F., GLEDENIN, L.F., BENTLEY, W.C. & ESSLING, A.M. (1971): Precision measurements of half-lives and specific activities of ^{235}U and ^{238}U. *Phys. Rev.* **C4**, 1889-1906.

LAN, CHING-YING, CHUNG, SUN-LIN, LO, CHING-HUA, LEE, TUNG-YI, WANG, PEI-LING, LI, HUIMIN & VAN TOAN, DINH (2001): First evidence for Archean continental crust in northern Vietnam and its implications for crustal and tectonic evolution in south-east Asia. *Geology* **29**, 219-222.

________, ________, SHEN, JIUN-SAN, LO, CHING-HUA, WANG, PEI-LING, HOA, TRAN-TRONG, THANH, HPANGHUU & MERTZMAN, S.A. (2000): Geochemical and Sr–Nd isotopic characteristics of granitic rocks from northern Vietnam. *J. Asian Earth Sci.* **18**, 267-280.

LEAKE, B.E., WOOLLEY, A.R., ARPS, C.E.S., BIRCH, W.D., GILBERT, M.C., GRICE, J.D., HAWTHORNE, F.C., KATO, A., KISCH, H.J., KRIVOVICHEV, V.G., LINTHOUT, K., LAIRD, J., MANDARINO, J.A., MARESH, W.V., NICKEL, E.H., ROCK, N.M.S., SCHUMACHER, J.C., SMITH, D.C., STEPHENSON, N.C.N., UNGARETTI, L., WHITTAKER, E.J.W. & GUO, YOUZHI (1997): Nomenclature of amphiboles: report of the Subcommittee on Amphiboles of the International Mineralogical Association, Commission on New Minerals and Mineral Names. *Can. Mineral.* **35**, 219-246.

________, ________, BIRCH, W.D., BURKE, E.A.J., FERRARIS, G., GRICE, J.D., HAWTHORNE, F.C., KISCH, H.J., KRIVOVICHEV, V.G., SCHUMACHER, J.C., STEPHENSON, N.C.N. & WHITTAKER, E.J.W. (2003): Nomenclature of amphiboles: additions and revisions to the International Mineralogical Association's 1997 recommendations. *Can. Mineral.* **41**, 1355-1362.

LELOUP, P.H., ARNAUD, N., LACASSIN, R., KIENAST, J.R., HARRISON, T.M., PHAN TRONG, TRINH, REPLUMAZ, A. & TAPPONNIER, P. (2001): New constraints on the structure, thermochronology, and timing of the Ailao Shan – Red River shear zone, SE Asia. *J. Geophys. Res.* **106**, 6683-6732.

________, HARRISON, T.M., RYERSON, F.J., CHEN, WENJI, LI, QI, TAPPONNIER, P. & LACASSIN, R. (1993): Structural, petrological and thermal evolution of a tertiary ductile strike-slip shear zone, Diancang Shan, Yunnan. *J. Geophys. Res.* **98**, 6715-6743.

________, LACASSIN, R., TAPPONNIER, P., SCHÄRER, U., ZHONG, DALAI, LIU, XIAOHAN, ZHANG, LIANSHANG, JI, SHAOCHENG & PHAN TRONG, Trinh (1995): The Ailao Shan – Red River shear zone (Yunnan, China), Tertiary transform boundary of Indochina. *Tectonophysics* **251**, 3-84.

________, ROGER, F., JOLIVET, L., LACASSIN, R., PHAN TRONG, TRINH, BRUNEL, M. & SEWARD, D. (1999): Unravelling a long and complex thermal history by multi-system geochronology: example of the Song Chay metamorphic dome, north Vietnam. *Terra Abstr. EUG* **10**, 433.

LEPVRIER, C., MALUSKI, H., VUONG, NGUYEN VAN, ROQUES, D., AXENTE, V. & RANGIN, C. (1997): Indosinian NW-trending shear zones within the Truong Son belt (Vietnam): ^{40}Ar–^{39}Ar Triassic ages and Cretaceous to Cenozoic overprints. *Teconophysics* **283**, 105-127.

LI, SHUGUANG, XIAO, YILIN, LIOU, DELIANG, CHEN, YIZHI, GE, NINGJIE, ZHANG, ZONGQING, SUN, SHEN-SU, CONG, BOLIN, ZHANG, RUYUANG, HART, S.R. & WANG, SONGSHAN (1993): Collision of the North China and Yangtse blocks and formation of coesite-bearing eclogites: timing and processes. *Chem. Geol.* **109**, 89-111.

MALUSKI, H., LEPVRIER, C., JOLIVET, L., CARTER, A., ROQUES, D., BEYSSAC, O., TRONG TANG, TA, NGUYEN DUC, TANG & AVIGAD, D. (2001): Ar–Ar and fission-track ages in the Song Chay Massif: early Triassic and Cenozoic tectonics in northern Vietnam. *J. Asian Earth Sci.* **19**, 233-248.

________, ________, TRONG TANG, TA & NGUYEN DUC, TANG (1999): Effect of up-doming process in the Song Chay Massif (Vietnam) on Ar–Ar ages. *Terra Abstr. EUG* **10**, 57.

NAM, T.N., TORIUMI, M. & ITAYA, T. (1998): P–T–t paths and post-metamorphic exhumation of the Day Nui Con Voi shear zone in Vietnam. *Tectonophysics* **290**, 299-318.

PÊCHER, A., GIULIANI, G., GARNIER, V., MALUSKI, H., KAUSAR, A.B., MALIK, R.H. & MUNTAZ, H.R. (2002): Geology, geochemistry and Ar-Ar geochronology of the Nangimali ruby deposit area, Nanga–Parbat Himalaya (Azra Kashmir, Pakistan). *J. Asian Earth Sci.* **21**, 265-282.

PHAM VAN, L, HOÀNG QUANG, VINH, GARNIER, V., GIULIANI, G. & OHNENSTETTER, D. (2004): Marble-hosted ruby from Vietnam. *Can. Gemmologist* **25**, 83-95.

PHAN TRONG, T. & HOÀNG QUANG, V. (1997): So Dô Kiên Tao Vunh Luc Yên. Geological map of Luc Yen. Institute of Geological Sciences, Hanoi, Vietnam (scale 1 : 200,000).

________, LELOUP, P.H., ARNAUD, N. & LACASSIN, N. (1998): Formation of ruby in the Red river metamorphic zone. *Proc. Nat. Centre for Natural Sciences and Technology* **10**(1), 143-148.

POUCHOU, J.L. & PICHOIR, F. (1991): Quantitative analysis of homogeneous or stratified microvolumes applying the model "PAP". *In* Electron Probe Quantitation (K.F.J. Heinrich & D.E. Newbury, eds.). Plenum Press, New York, N.Y. (31-75).

ROGER, F., LELOUP, P.H., JOLIVET, L., LACASSIN, R., PHAN TRONG, TRINH, BRUNEL, M. & SEWARD, D. (2000): Long and complex thermal history of the Song Chay metamorphic dome (northern Vietnam) by multi-system geochronology. *Tectonophysics* **321**, 449-466.

SCHÄRER, U., TAPPONNIER, P., LACASSIN, P.H., LELOUP, P.H., ZHONG, D. & JI, S. (1990): Intraplate tectonics in Asia: a precise age for large-scale Miocene movement along the Ailao Shan – Red River shear zone, China. *Earth Planet. Sci. Lett.* **97**, 65-77.

________, ZHANG, LIAN-SHENG & TAPPONNIER, P. (1994): Duration of strike-slip movements in large shear-zones: the Red River belt, China. *Earth Planet. Sci. Lett.* **126**, 379-397.

STACEY, J.S. & KRAMERS, J.D. (1975): Approximation of terrestrial lead isotope evolution by a two stage model. *Earth Planet. Sci. Lett.* **26**, 207-221.

TAPPONNIER, P., LACASSIN, R., LELOUP, P.H., SCHÄRER, U., ZHONG, DALAI, LIU, XIAOHAN, JI, SHAOCHEN, ZHANG, LIANSHANG & ZHONG, JIAYON (1990): The Ailao Shan/Red River metamorphic belt: Tertiary left-lateral shear between Indochina and south China. *Nature* **343**, 431-437.

WIEDENBECK, M., ALLÉ, P., CORFU, F., GRIFFIN, W.L., MEIER, M., OBERLI, F., VON QUADT, A., RODDICK, J.C. & SPIEGEL, W. (1995): Three natural zircon standards for U–Th–Pb, Lu–Hf, trace elements and REE analyses. *Geostandard Newslett.* **19**, 1-23.

ZHANG, LIAN-SHENG & SCHÄRER, U. (1999): Age and origin of magmatism along the Cenozoic Red River shear belt, China. *Contrib. Mineral. Petrol.* **134**, 67-85.

Received May 29, 2003, revised manuscript accepted November 25, 2004.